Tellus (1995), 47A, 834–848
Printed in Belgium – all rights reserved

Copyright © Munksgaard, 1995
TELLUS
ISSN 0280–6495

Origin and structure of a numerically simulated polar low over Hudson Bay

By MARK D. ALBRIGHT, RICHARD J. REED*, *Department of Atmospheric Sciences, AK-40, University of Washington, Seattle, WA 98195, USA*, and DAVID W. OVENS, *Olympia Weather Service Office, National Weather Service, 7645 Old 99 Highway SE, Olympia, WA 98501, USA*

(Manuscript received 29 August 1994; in final form 14 February 1995)

ABSTRACT

The PSU-NCAR mesoscale model (MM4) is used to simulate a polar low that developed over Hudson Bay in December 1988. The structure and characteristics of the simulated low are documented, and results are presented of sensitivity experiments aimed at elucidating the physical mechanisms involved in the cyclogenesis. The low formed over an ice-free region in the eastern bay as an amplifying upper-level cold trough advanced into the region. The model depicted the polar low as a small, relatively shallow system embedded within the larger cold low. It resembled a miniature hurricane in structure but lacked hurricane-force winds. The lapse rate near its center was moist neutral to 550 mb (4 km); anticyclonic outlow occurred at and immediately below that level. The sensitivity experiments revealed that fluxes of heat and moisture from the region of open water and the associated condensation heating in deep organized convection were essential to the development. Sensible heating alone produced a relatively weak low and no low formed in an experiment with a completely ice-covered bay. The feedback between the surface fluxes and wind speed enhanced the intensification, especially in an experiment with the sea surface temperature raised by 8°C. Winds of minimal hurricane intensity were attained in the latter experiment when the feedback effect was included but not when it was disallowed. A sizable impact of the ice-edge configuration was found. It is concluded that the Hudson Bay polar low formed as a consequence of latent heat release in deep organized convection that formed when an upper-level cold low moved over a relatively warm body of open water from which large fluxes of heat and moisture took place. Baroclinic forcing appeared to play little direct role in the low development. Instead, the configuration of the upstream ice boundary provided an important initiating and organizing mechanism.

1. Introduction

Roch et al. (1991) reported on a polar low that formed over an ice-free region in eastern Hudson Bay (Fig. 1) in early December 1988. They described the results of numerical simulations of the low performed with a high-resolution version of the Canadian operational regional finite-element model (RFE). The object of their experiments was to test the sensitivity of the development to horizontal resolution and to ice cover. Experiments were run at 100-km, 50-km, and 25-km grid resolutions and with four different ice covers: those given by (1) the operational analysis, (2) a refined analysis from Environment Canada's Ice Centre, (3) an assumed complete ice cover, and (4) an assumed complete absence of ice. The most realistic simulation of the low was obtained from the experiment with the 25-km grid and the ice-cover analysis of Environment Canada's Ice Centre. The importance of the open water to the formation of the simulated low was indicated by the failure of a closed low to form in the experiment with complete ice cover.

In the present paper the Pennsylvania State University-National Center for Atmospheric Research (PSU-NCAR) mesoscale model, version

* Corresponding author.

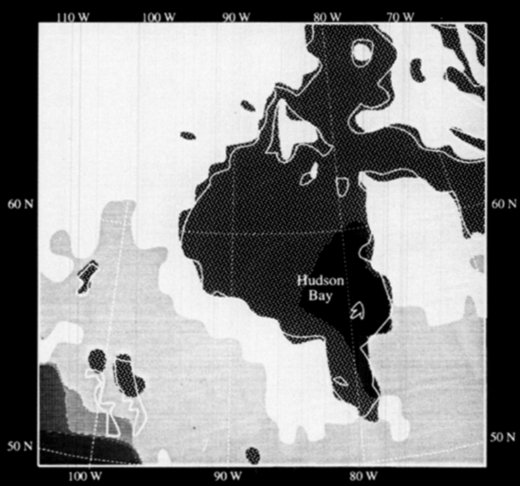

Fig. 1. Model domain for experiments HB1–HB8 (HB, Hudson Bay). Stippled region over the sea indicates the presence of sea ice. Remaining stippling indicates other land-use categories.

IV (MM4) is used to expand on the earlier results of Roch et al. (1991). Information is presented on a number of features of interest that were not shown in their paper, including the vertical structure of the simulated low, the fields of surface sensible and latent heat flux, the precipitation distribution and amounts, and the pattern of vertical motion. In addition an expanded set of sensitivity experiments is conducted, aimed at better understanding the physics of polar low formation in this and similar cases. In particular, the experiments will test the sensitivity of the development to various prescriptions of the surface fluxes, to condensation heating, to sea-surface temperature, and to the configuration of the ice boundary.

A brief description of the synoptic background is given in Section 2. Section 3 contains a description of the MM4 model and the sensitivity experiments that were conducted. Results of the structural and diagnostic studies and of the sensitivity tests are found in Section 4. The final section summarizes and discusses the main conclusions.

2. Synoptic background

Salient features of the development are shown in Fig. 2 which depicts surface and 500 mb charts at 0000 UTC 8 December prior to the polar low event (Figs. 2a, c, respectively), and at 1200 UTC 9 December (Figs. 2b, d) close to the time of maximum development. At the earlier hour a broad current of Arctic air with upstream surface temperatures in the range $-25°C$ to $-30°C$ was flowing southeastward across Hudson Bay (Fig. 2a). Aloft (Fig. 2c) a series of short-wave troughs encircled a low centered over Baffin Island. Of special significance is the short-wave trough on the northwest shore of Hudson Bay (heavy, dashed line). During the subsequent 36 hours this trough amplified, forming a closed low over southern Hudson Bay (Fig. 2d). As it did so, a small intense surface low appeared over the open water adjacent to the east shore of the bay (Fig. 2b). The position and central pressure (997 mb), as shown, are subject to some uncertainty, but the presence of an intense system is beyond doubt, as evident from data at the shore station labeled I and from satellite imagery (Roch et al., 1991). It is of interest to note that temperatures at this station were 20°C warmer than in the upstream flow, reflecting the presence of the nearby open water.

3. Model and experiments

The model employed here, the PSU-NCAR Mesoscale Model, Version IV (MM4), is a hydrostatic, primitive equation model that utilizes a terrain-following sigma coordinate. Physics of the model include an explicit scheme for grid-resolvable precipitation (Hsie et al., 1984); convective parameterization by the Arakawa-Schubert (1974) scheme, as modified by Grell (1993); the Blackadar (1979) high-resolution scheme for boundary-layer processes; fourth-order deformation-dependent horizontal diffusion; and second-order, Richardson number-dependent vertical diffusion. All experiments were run on a 20-km horizontal grid with 28 sigma levels in the vertical for a period of 30 h commencing at 1200 UTC 8 December 1988. With minor modification to be noted below, the initial analyses were obtained from coarse NMC gridded data reanalyzed to the mesoscale grid with use of available surface and upper-air data. Water temperatures were also supplied by NMC analyses. Ice cover (Fig. 1), except when otherwise specified, was patterned after the analysis of Environment Canada's Ice Centre,

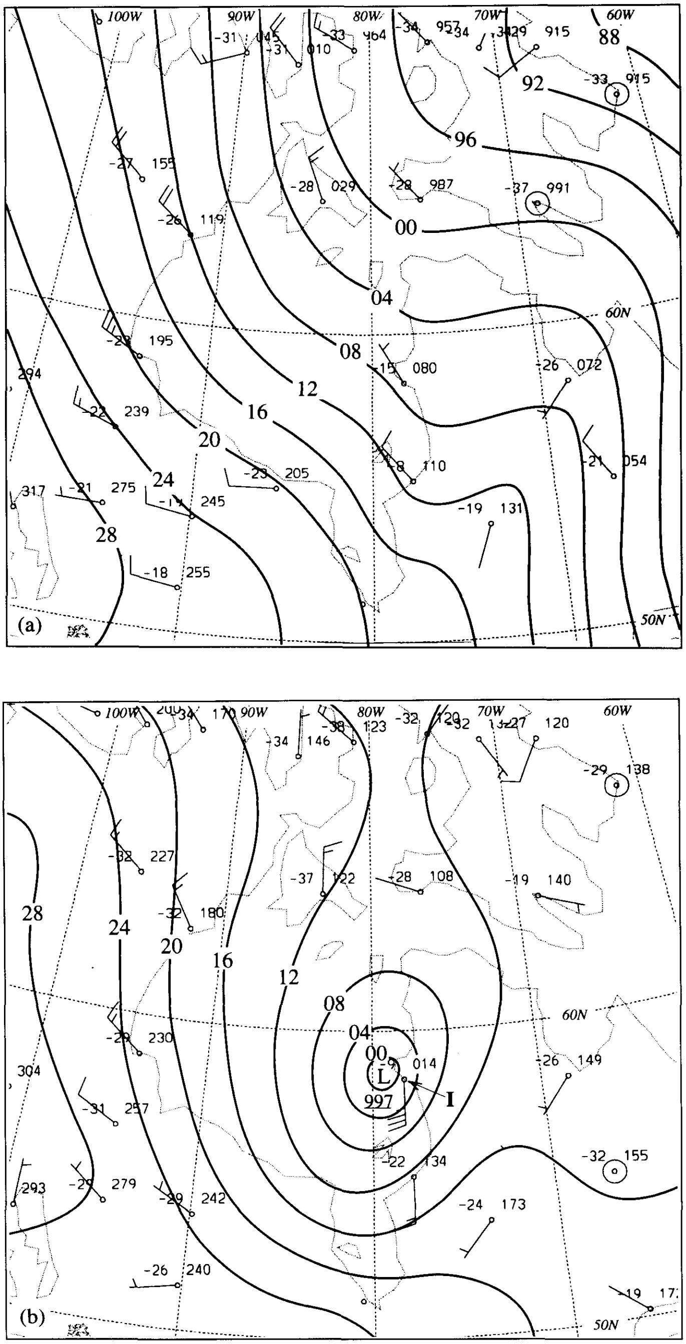

Fig. 2. NMC surface and 500 mb analyses for 0000 UTC 8 December 1988 and 1200 UTC 9 December 1988. (a) Surface and (c) 500 mb for 0000 UTC 8 December; (b) and (d) same for 1200 UTC 9 December. The I in (b) denotes the Inukjuak station. The heavy dashed line in (c) indicates the short-wave trough on the northwest shore of Hudson Bay.

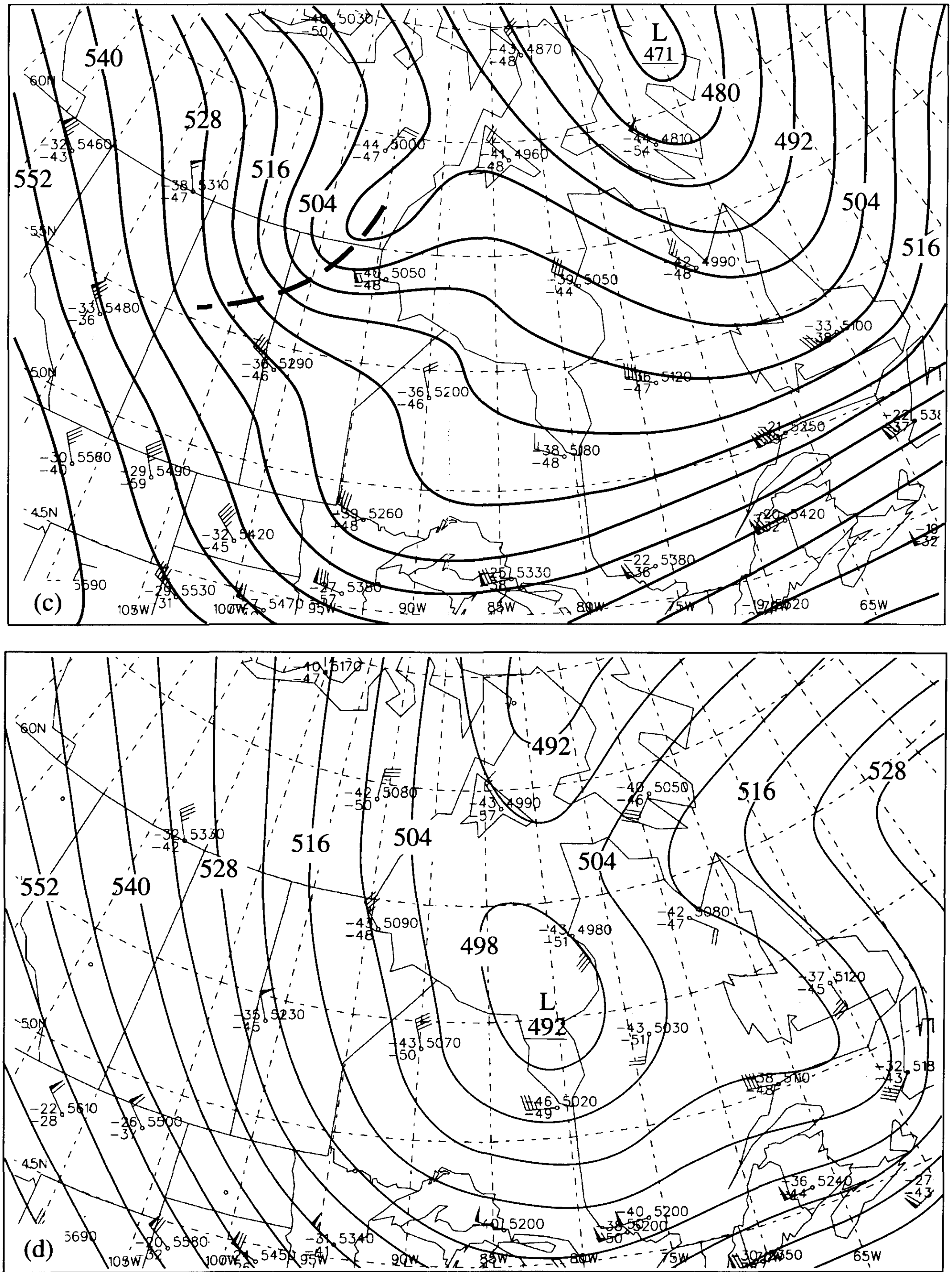
(c)
L
471
480
492
504
516
528
540
552
60N
55N
50N
45N
105W
100W
95W
90W
85W
80W
75W
65W
(d)
492
528
516
504
498
L
492
552
540
528

Fig. 2. (cont'd).

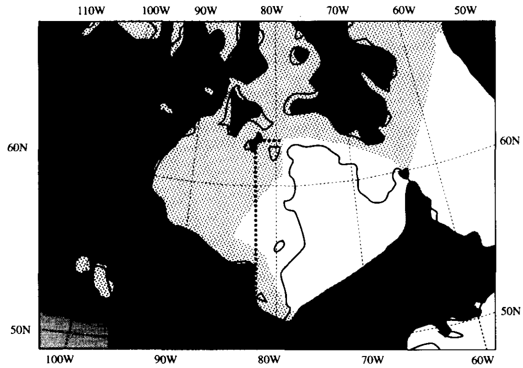

Fig. 3. Model domain for experiments HB9 and HB10 with artificial ice-free sea extended across northern Quebec. Stippling same as in Fig. 1. Western boundary in HB9 is given by the lightest stippling and in HB10 by heavy dotted line.

as shown in Roch et al. (1991). The first eight experiments were carried out on the 113 × 113 grid domain shown in Fig. 1; the final two experiments were conducted on the larger 113 × 155 grid domain depicted in Fig. 3. Time-dependent lateral boundary conditions were obtained by interpolation from 12-hourly NMC analyses.

A summary of the ten experiments that were conducted appears in Table 1. The first experiment HB1, the control experiment, utilized the full model physics and observed ice cover. Initial conditions over eastern Hudson Bay were subjectively modified to bring the initial analyses in the open water region into agreement with the Inukjuak (location I in Fig. 2b) radiosonde observation. HB2 differed from the control in specifying a fully ice-covered bay. A subjective procedure was employed to replace the boundary-layer structure in the MM4 reanalysis of the NMC gridded data, which contained the effects of prior fluxes from the open water, by a structure more appropriate for an experiment that assumes a preexisting full ice cover. The procedure consisted of (1) removing the Inukjuak sounding from the data analyses and also removing surface observations from two nearby stations that clearly showed the effects of the open water, (2) reinserting at the location of Inukjuak a bogus sounding that was identical to the original sounding above 800 mb and isothermal below, and (3) bogusing low-level temperatures at 27 additional points over the ice-free portion of Hudson Bay, essentially creating isothermal profiles below 800 mb at these locations as well. Basically HB2 is a no-flux experiment, since surface fluxes in this experiment were found to be small compared to those in the control run. HB3 repeated the control run with the altered boundary layer of HB2. This experiment tests the extent to which the development in the control run depended on the heating and moistening of the atmosphere by prior fluxes as opposed to the effects of the fluxes occurring during the course of the simulation.

Experiment HB4 is similar to the control experiment except that it does not allow the wind speed in the surface flux formulas to exceed 5.9 m s^{-1}, the mean wind speed over the model domain during the complete ice cover (HB2) simulation. This procedure gives a measure of the importance of the feedback between wind speed and fluxes in storm intensification (Emanuel and Rotunno, 1989). In experiment HB5 surface sensible heat

Table 1. *Summary of experiments*

Name	30-h central pressure (mb)	SST (°C)	Size of ice-free region (km^2)	Surface fluxes sensible	Surface fluxes latent	Latent heating	Brief description
HB1	997	0°C	200,000	yes	yes	yes	control, observed ice cover
HB2	—	—	0	yes	yes	yes	complete ice cover
HB3	997	0°C	200,000	yes	yes	yes	no initial PBL modification
HB4	1003	0°C	200,000	limited		yes	limited surface fluxes
HB5	1006	0°C	200,000	yes	no	yes	no latent heat flux
HB6	1006	0°C	200,000	yes	yes	no	no latent heating
HB7	981	8°C	200,000	yes	yes	yes	enhanced SST
HB8	996	8°C	200,000	limited		yes	enhanced SST, limited fluxes
HB9	995	0°C	700,000	yes	yes	yes	enlarged ice-free region
HB10	1001	0°C	700,000	yes	yes	yes	enlarged sea, straight ice-edge

flux is allowed but not surface latent heat flux. This experiment tests the ability of sensible heating alone to develop a polar low under the given circumstances. A reverse experiment was conducted in which latent heat flux was allowed but not sensible heat flux. In this case multiple, very weak lows formed that could not be associated with the system of interest. Accordingly, the experiment is not assigned a number and will not be further discussed. In HB6 latent heating is suppressed thereby testing its effect on the low development. Moisture is carried as a passive variable but is not allowed to produce heating when condensed.

In HB7, the SST of the ice-free area was increased from 0°C, the value in the control run, to 8°C for the purpose of testing the effect of water temperature on the structure and intensity of the polar low. HB8 repeats HB7 but with the suppression of the wind-surface-flux feedback effect in the manner done in HB4. In HB9, the ice-free area of Hudson Bay is enlarged eastward and northward (Fig. 3) to create a water body comparable in size to the Greenland and Norwegian Seas. The purpose is to test whether the location, size, and intensity of the low at 30 hours would have differed significantly had the same synoptic conditions prevailed near an extended ice edge bordering a large sea rather than near a small, confined body of open water. Finally, HB10 repeats HB9 but with the indented western ice boundary (Fig. 3) replaced by the straight ice boundary given by the dotted line in that figure. This experiment provides a test of the sensitivity of the development to the configuration of the ice edge.

4. Results

4.1. Structure and characteristics of the development in the control (full physics) simulation and comparison with results of the complete ice-cover simulation

Shown in Fig. 4 are the initial surface and 500 mb maps at 1200 UTC 8 December (a, c), and the predicted surface and 500 mb maps at 30 hours (1800 UTC 9 December) for the control run (b, d). The initial surface map for the run with complete ice cover appears in Fig. 5a, and the predicted surface and 500 mb maps at 30 h for this run appear in Figs. 5b, c. The isobaric pattern at the initial time (Fig. 4a) is similar to that observed 12 h earlier (Fig. 2a) except that a more pronounced trough is present over the region of open water. The 30-h simulated surface pressure field (Fig. 4b) exhibits a general rise in pressure over ice-covered portions of Hudson Bay and the appearance of a small, intense cyclone over the ice-free region. The depth of the low is similar to that of the observed low 6 hours earlier (Fig. 2b) while its location is somewhat farther south. The initial surface chart in the ice-covered experiment features the expected colder temperatures in eastern Hudson Bay resulting from the removal of the warm anomaly. Without this anomaly, and in the absence of subsequent surface energy fluxes of appreciable size, no surface low formed during the 30 h simulation (Fig. 5b).

The location and depth of the low in the control experiment are plotted at 6-h intervals in Fig. 6. The low first appeared over the coastal waters near 60° N, 80° W with a central pressure of 1007 mb. Subsequently it moved or redeveloped southward in the offshore region and reached a depth of 997 mb a short distance to the northeast of the Belcher Islands at hour 30. The position and depth at 24 h are similar to those obtained by Roch et al. (1991) in an experiment with open water and a 25-km grid (see their Fig. 11c).

Because of the paucity of data in the region of formation, the behavior of the actual low, as stated previously, is uncertain. Roch et al. (1991) have utilized satellite imagery to deduce the likely position of the low center and on this basis inferred that a dual development took place with the later low forming farther to the south than the earlier. Thus, the tendency of the low in the simulation to move southward by discrete steps bears some resemblance to the observed behavior. Because of the foregoing uncertainties, it cannot be claimed that the simulation perfectly recreates the actual event(s). However, there can be no doubt, on the basis of a reported 1001 mb surface pressure and simultaneous wind speed of 22 m s^{-1} at Inukjuak at 1300 UTC 9 December, five hours earlier than the map shown in Fig. 4b, that a polar low of approximately the same strength as the simulated low appeared in nearly the same location at nearly the same time.

The initial 500 mb chart (Fig. 4c) shows that the upper-level, short-wave trough amplified in the 12 h period between 0000 UTC and 1200 UTC

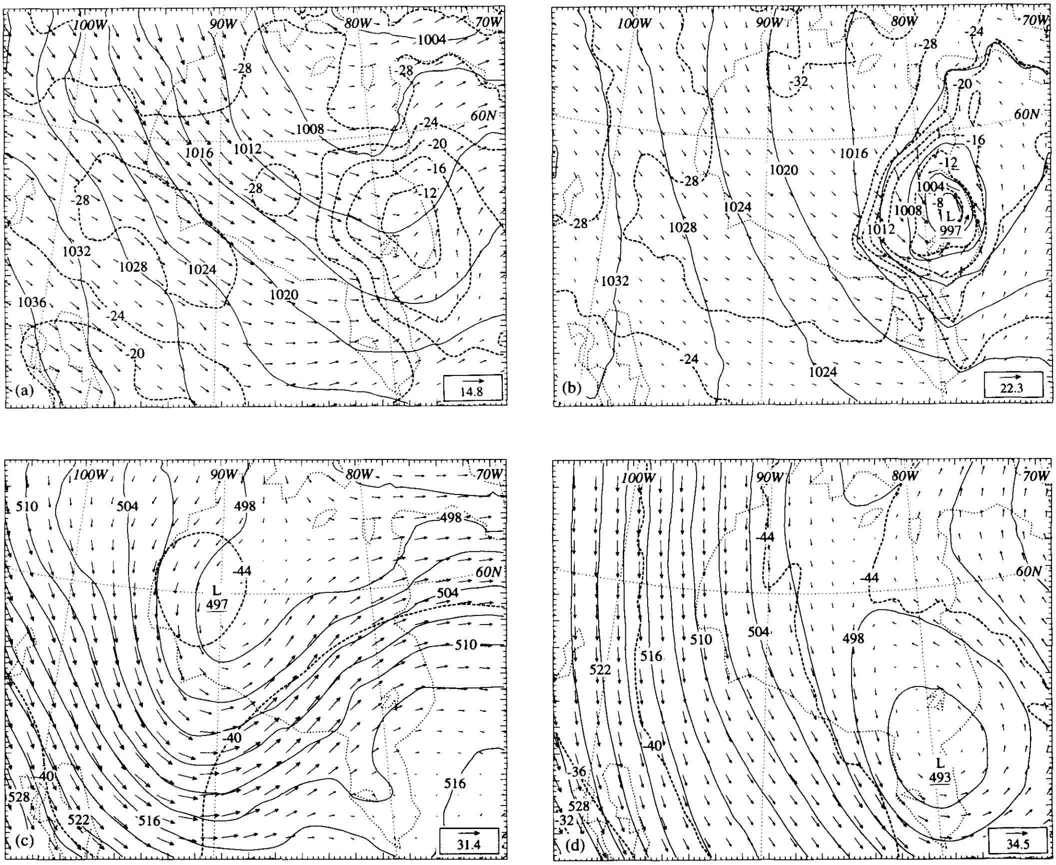

Fig. 4. Surface pressure at 4 mb interval (solid line), temperature at 4°C interval (dashed line) and vector wind in $m\ s^{-1}$ at (a) initial hour, 1200 UTC 8 December, and (b) 30-h forecast time, 1800 UTC 9 December, for control run HB1 and corresponding 500 mb charts (c) and (d) of geopotential height at 3 dam interval, temperature at 4°C interval, and winds ($m\ s^{-1}$). Wind velocity scales at lower right of each map.

8 December (compare with Fig. 2b). The amplification continued during the forecast period so that by 30 hours (Fig. 4d) a closed low had appeared over southern Hudson Bay. The geopotential heights are remarkably similar to those observed at 1200 UTC 9 December (Fig. 2d). The 500 mb chart for the ice-covered case (Fig. 5c) resembles closely that of the control run. Minor differences are apparent near the center of the upper-level vortex where heights are slightly lower, and the cyclonic circulation is somewhat stronger in the ice-covered case. The smaller 500 mb height deficit in the control run is likely a manifestation of the warmer lower atmosphere in that run and the presence, as shown below, of anticyclonic outflow at intermediate levels.

Intermediate-level 850 mb and 700 mb charts (Figs. 7a, b) reveal that the upper and lower vortices are discrete entities. The surface vortex weakens upward along the vertical so that by 700 mb only a weak height minimum and temperature maximum remain. South of the 700 mb low center a weak high pressure system and pronounced, divergent anticyclonic outflow are in evidence. A similar outflow was noted by Nordeng and Rasmussen (1992) in a previous polar low simulation. The existence of the divergent outflow at 700 mb is consistent with the presence of a level

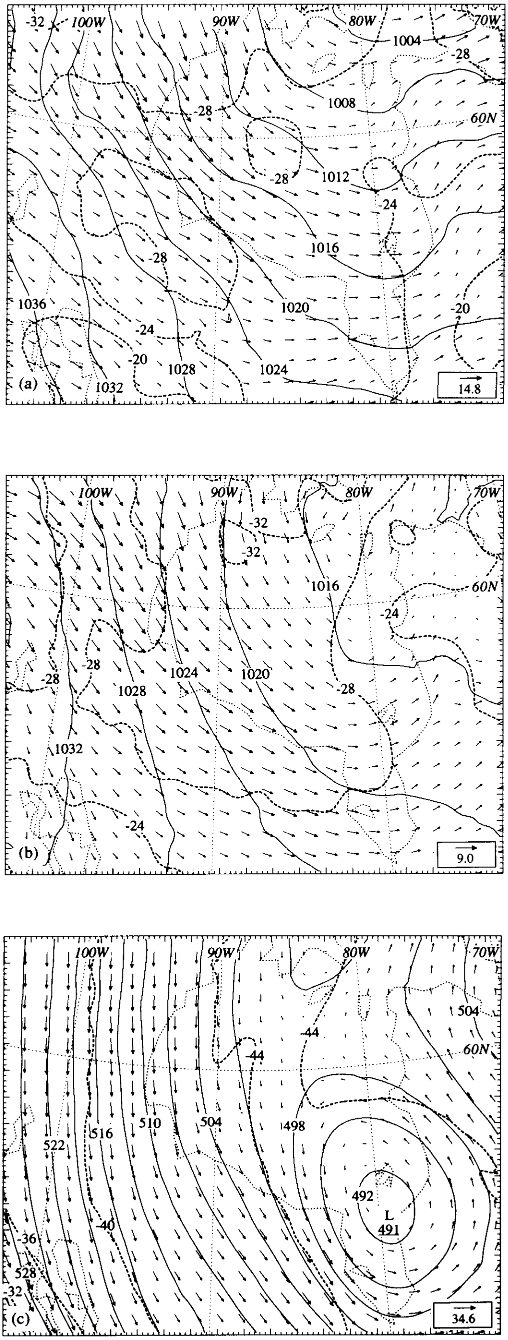

Fig. 5. As in Fig. 4 for the ice-covered experiment, HB2, except that panel (c) shows the 30-h forecast at 500 mb. The initial 500 mb analysis is the same as that shown in Fig. 4c and is not repeated.

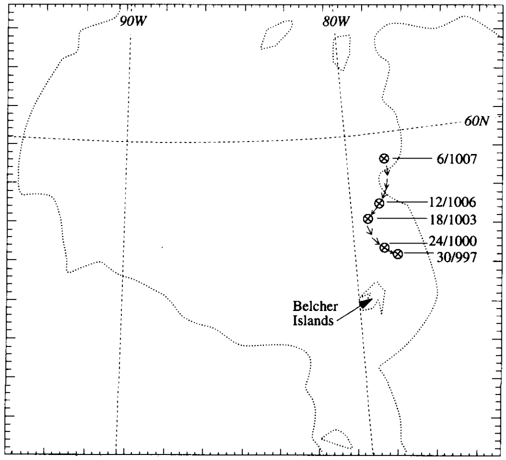

Fig. 6. Six-hourly positions and central pressures of the polar low simulated in the control run (HB1).

of neutral buoyancy near 600 mb for parcels rising from low levels as shown by the sounding in Fig. 8 (solid lines), and by the rapid decline in upward velocities (right margin), and associated vertical mass convergence below that level. The location of the sounding in Fig. 8 is marked by the dot near the low center in Fig. 7a. Also shown in Fig. 8 is the sounding (dotted lines) for the same point in the ice-covered case. Comparison of the two soundings illustrates well the heating of the lower atmosphere produced by the fluxes.

An idea of the magnitude of the fluxes that were produced in the model simulation is afforded by Fig. 9, which maps average values for the 6-h period between 24 and 30 hours when surface winds were strongest and therefore represent upper limits. Sensible heat fluxes (Fig. 9a) as large as 1315 W m^{-2} and latent heat fluxes (Fig. 9b) as large as 305 W m^{-2} were present near the upwind ice-edge during the period. In the vicinity of the polar low, sensible heat fluxes ranged from 100–500 W m^{-2} and latent heat fluxes from 50–200 W m^{-2}.

The 30-h cumulative precipitation is shown in Fig. 10a. Prominent features are an elongated region of maximum values that extends southward just to the east of 80° W and then westward, a second elongated region of lesser amounts that lies close to the east shore along its middle and lower portions, and a corridor of minimum amounts that

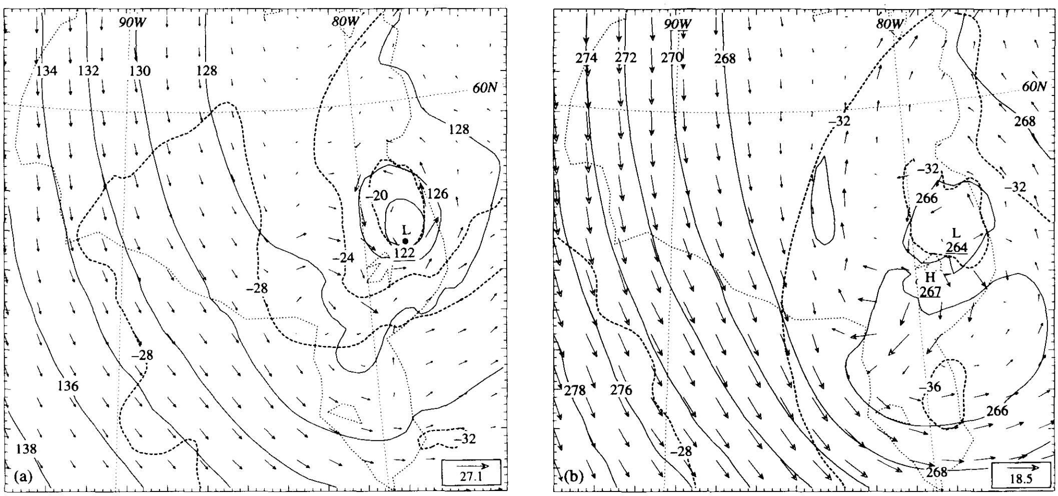

Fig. 7. Upper-level charts for 1800 UTC 9 December. Solid lines, geopotential height at 2 dam interval; dashed lines, temperature at 4°C interval; vector winds in m s^{-1}, scale at lower right. (a) 850 mb. L denotes low center and dot indicates position of soundings in Fig. 8. (b) 700 mb.

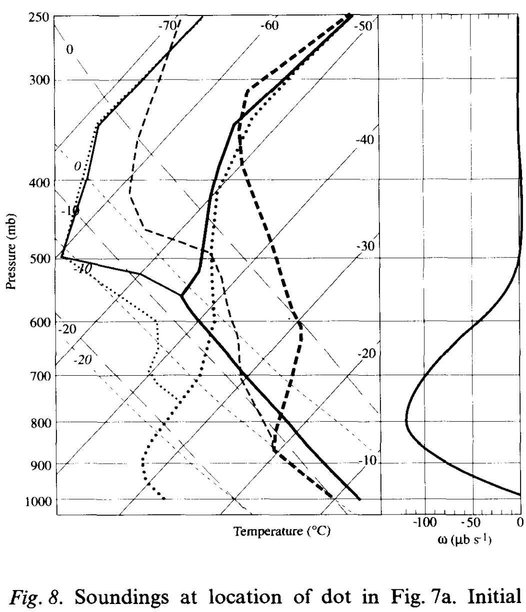

Fig. 8. Soundings at location of dot in Fig. 7a. Initial temperature (heavy dashed) and dew point (medium dashed) at 1200 UTC 8 December for HB1. Final temperature (heavy solid) and dew point (medium solid) for 1800 UTC 9 December for HB1. Final temperature (large dots) and dew point (small dots) for HB2. Isotherms: thin slanting solid lines. Dry adiabats: pecked lines. Saturated adiabats: thin dashed. Curve at right depicts omega profile in μb s^{-1}.

separates the two bands. Maximum amounts are 23.2 mm in the first band and 9.5 mm in the second. The minimum value in the dry corridor is less than a millimeter. Because of the relatively small movement of the polar low, individual patterns for shorter periods (not shown) bear a close resemblance to the overall pattern. It is also worthy of note that 100% of the indicated precipitation stemmed from grid-resolvable precipitation rather than from subgrid-scale precipitation. Evidently, under the highly unstable conditions that prevailed, grid points became almost immediately saturated on the 20-km grid-scale.

Fig. 8 provides an example (solid curve) of conditions at a grid point where resolvable-scale precipitation is occurring. The sounding at the point is moist neutral to 570 mb, and the vertical motion is of the order of 1 m s^{-1}. We regard these conditions to be indicative of deep convection of mesoscale dimensions and henceforth when referring to model output will use the term deep convection to denote convection on this scale.

From Fig. 10b, it is apparent that the vertical motion pattern at 850 mb is similar to the precipitation pattern. For the purpose of eliminating transient features, the vertical motion is depicted by average values for the 6-h period from 24 to 30 h when the motions are fully developed. Strongest

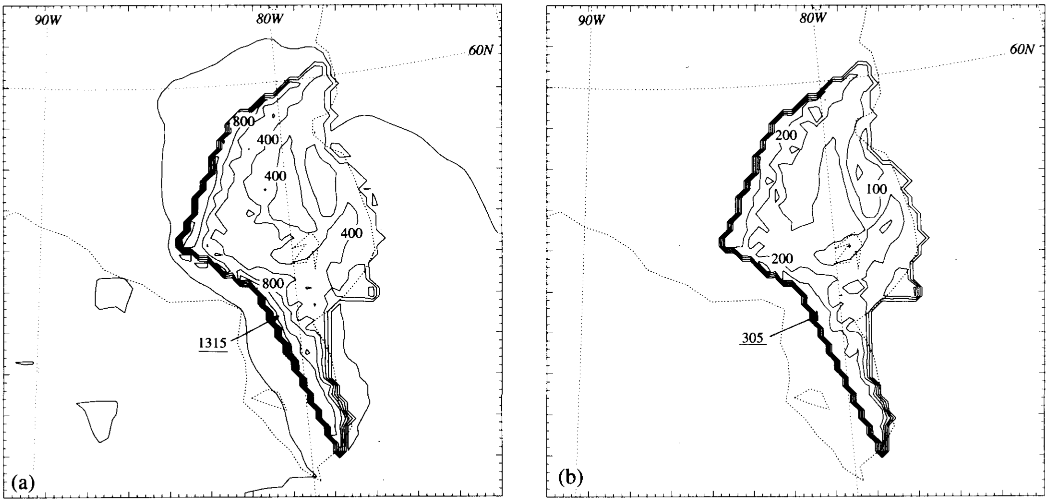

Fig. 9. Time averaged surface energy fluxes (W m^{-2}), hours 24 to 30. (a) Sensible heat flux. (b) Latent heat flux. Contour intervals are 200 W m^{-2} in (a) and 50 W m^{-2} in (b).

upward motions (peak value $-83\,\mu b\,s^{-1}$) occur in the offshore major precipitation band. A long, broken belt of lesser upward motions is located near the shoreline. A corridor of descending motion or weak upward motion lies between. Some sinking motions also occur on the outer sides of the belts of ascent. An examination of 3-hourly surface charts (not shown) reveals that early in the experiment, convergence lines formed near the ice edge and along the east shore of Hudson Bay. The line from the ice edge moved eastward rapidly and became the main zone of activity. The line along the east shore remained nearly stationary.

4.2. *Sensitivity tests*

The traces of central pressure of the surface low are displayed in Fig. 11 for experiments HB1 and HB3-10. The curves commence at hour 3 of the simulations except those for HB9 and HB10

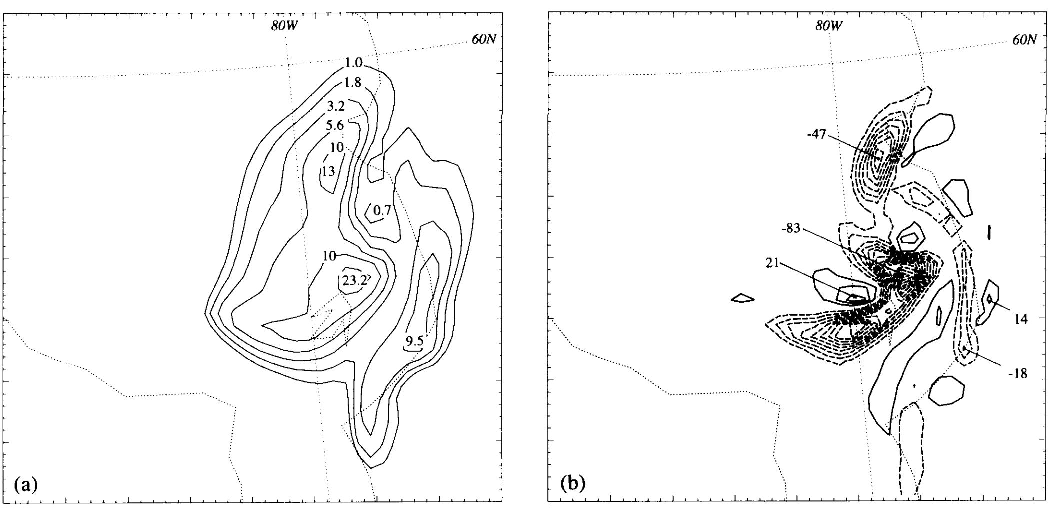

Fig. 10. (a) Cumulative precipitation in mm for 30-h period. Isohyets on logarithmic scale (b) Time-averaged 850-mb omega at intervals of $6\,\mu b\,s^{-1}$, hours 24 to 30. The solid (dashed) lines in (b) indicate positive (negative) values.

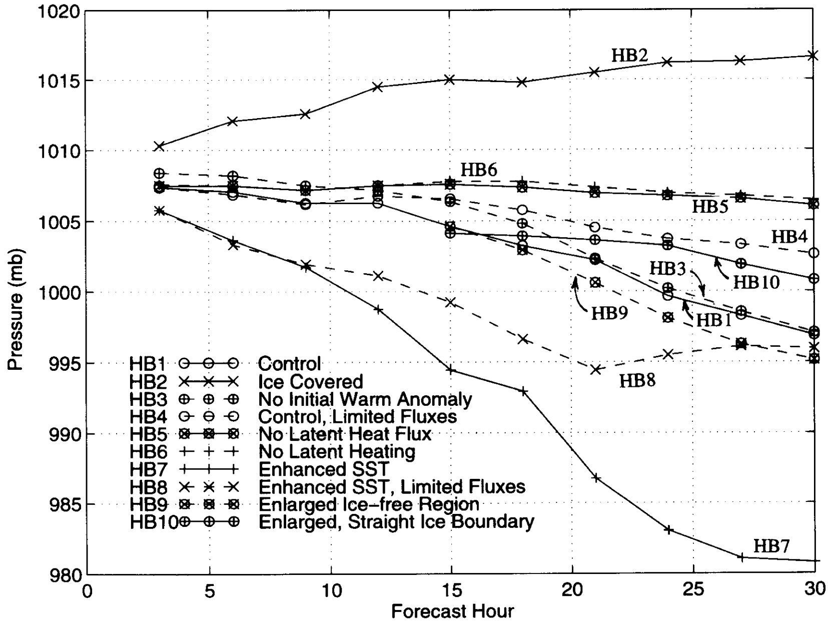

Fig. 11. Traces of central pressure for experiments HB1, HB3–HB10. See text for further explanation.

which begin at hour 15, the time when centers first appeared. For HB2, in which a low failed to develop, the curve depicts the change of surface pressure at the position of the low in experiment HB1. The curve is regarded as providing background pressures against which the deficit of pressure in the control experiment, and to a considerable degree in the other experiments, can be gauged.

The low in the control experiment formed at a pressure of 1007 mb and deepened only slightly during the first twelve hours of its existence. More rapid deepening then ensued, and a final pressure of 997 mb was achieved, as noted previously. The curve for HB3 follows closely that for HB1. From this it is concluded that preconditioning of the boundary layer had little effect on the development. Concurrent fluxes were sufficient to account for the system formed in the control run. Limiting the buildup of the fluxes with wind speed (HB4) resulted in a weaker system (1003 mb) and a delay in the start of the deepening. It is clear that the flux feedback mechanism had a substantial effect on the intensification. Shutting off the surface latent heat flux (HB5) allowed only an exceedingly weak low to form (final pressure 1006 mb). Evidently, the sensible heat flux alone was unable to produce a significant low. An almost identical weak development took place when latent heating was withheld (HB6). It can be inferred from the last two results that latent heating in clouds was inconsequential in the absence of surface moisture or latent heat flux despite the substantial sensible heat fluxes that existed. As in HB6, with the latent heating suppressed, only the sensible heating was available to aid the development. Evidently, to produce a vigorous polar low, surface sensible and latent heat fluxes must operate jointly to form deep precipitating clouds and thereby heat a substantial depth of the atmosphere.

An intense low, with a central pressure of 981 mb, formed in the experiment with enhanced SST (HB7). From the surface map shown in Fig. 12, it is seen that hurricane force winds ($>33\ \mathrm{m\,s^{-1}}$) occurred in the central region of the low. The maximum surface wind in this case is $34.5\ \mathrm{m\,s^{-1}}$. That the low also resembled a hurricane in other respects is seen from Fig. 13 in which the equivalent potential temperature, relative humidity and vertical velocity are displayed. A vertical system with an eye-like unsaturated inner core and a pressure thickness of greater than

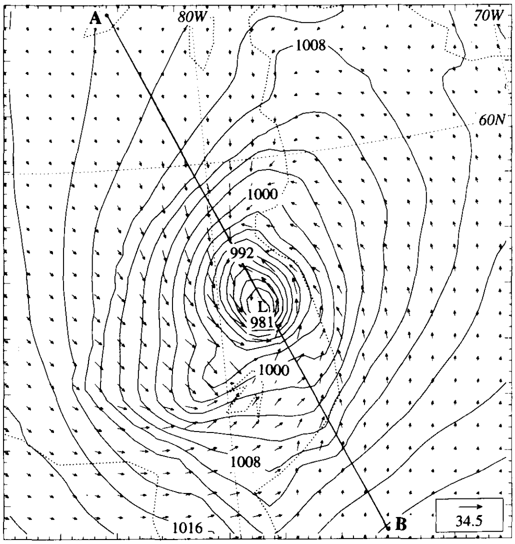

Fig. 12. Surface pressure at 27 h at 2 mb intervals and vector wind in m s^{-1} for the experiment HB7 with enhanced SST. Wind scale at lower right. Maximum wind 34.5 m s^{-1} (67 knots). Cross section for Fig. 13 is denoted by line AB.

600 mb (cloud tops near 350 mb) is evident. Sinking motions of about 30 μb s^{-1} in the "eye" are flanked by ascending motions as large as 154 μb s^{-1}) (1.7 m s^{-1}) in the surroundings. Emanuel and Rotunno (1989) have proposed the term "Arctic hurricanes" for polar lows. However, the results presented here suggest that only under extreme conditions is it possible to create winds of hurricane force. Thus it seems questionable to apply the term indiscriminately to polar lows, despite the structural similarities that may exist even in the weaker cases.

Experiment HB8, featuring limited fluxes in the enhanced SST case, shows an even more dramatic effect than in the experiments (HB1 and HB4) with the true SST. The lowest pressure attained is only 994.5 mb, and this occurs 6 h earlier than in the full-flux experiment. The maximum wind speed (not shown) is reduced to 23.7 m s^{-1}. These results lend further support to the Emanuel and Rotunno air-sea interaction instability (ASII) theory of polar-low intensification over Arctic seas.

In experiment HB9, with a large open sea to the east of the ice boundary, a low center failed to appear until 15 hours. The low that formed then deepened somewhat more rapidly than in the control experiment, reaching a pressure of 995 mb at 30 h. The position of the low, marked by the circled cross in Fig. 14, is somewhat farther south than in the control run. Evidently, displacement of the eastern boundary of the open water to a position far to the east had only a slight impact on the low development. Experiment HB10 with the straight ice boundary was run to test whether the similarity of the development in HB9 to that in HB1 was a consequence of employing the same

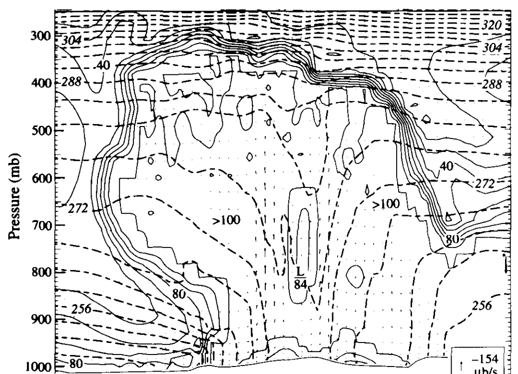

Fig. 13. Cross section of potential temperature at 4°C interval (dashed) and relative humidity at 10% interval (solid) along line AB in Fig. 12. Also shown are vertical motions in plane of cross section, scale at lower right.

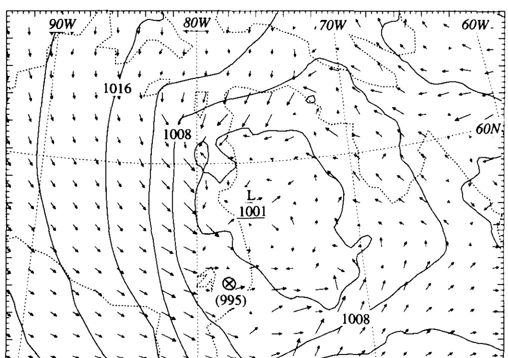

Fig. 14. 30-h forecast for experiment HB10. Isobars (solid) at 4 mb intervals; vector winds (m s^{-1}), scale at lower right. Circled cross indicates position of low center in HB9. Central pressure is plotted beneath.

shape for the western ice boundary in both experiments. Perhaps surprisingly, a large sensitivity to the shape was found, as can be seen from comparing the curves for HB9 and HB10 in Fig. 11. The 30-h surface chart for HB10 (Fig. 14) exhibits a considerably weaker low (1001 mb) than for HB9 and a more northerly position of the low center.

5. Concluding summary and discussion

From the foregoing results, it is concluded that the polar low under investigation was a moderately deep, vertical system, not unlike a small hurricane in structure, that owed its intensification to the flux of sensible and latent heat from the small region of open water that existed at the time in eastern Hudson Bay. An experiment conducted with an initially unmodified boundary layer led to the further conclusion that the fluxes occurring during the course of the development were sufficient to account for the final intensity of the system. Preheating and premoistening of the boundary layer had little effect on the outcome. No low formed in an experiment that specified a completely ice-covered bay and thereby effectively eliminated the surface energy fluxes.

A relatively weak low developed in an experiment in which latent heating was withheld. An identical weak low also formed in an experiment in which surface latent heat flux was suppressed but surface sensible heat flux and latent heating in clouds were retained. The similarity in the results of the two experiments leads to the conclusion that, in the absence of surface moisture flux, precipitation production was negligible so that only the effects of sensible heating were felt. In view of the much larger magnitude of the sensible heat flux (Bowen ratio of 3.0 to 4.0), it is perhaps surprising that sensible heating had so little impact when acting by itself.

The results summarized thus far highlight the central role that deep, organized convection plays in the development of the type of polar low under study. Fluxes of both sensible and latent heat are needed to produce deep convection, which in turn provides the condensation heating required for substantial intensification to occur. Observational studies have long stressed the importance of organized deep cumulus convection in connection with polar low formation, and many theoretical studies have assigned an essential role to it (Økland, 1987).

The dependence of flux intensity on wind speed was shown to have a substantial effect on the deepening. This was particularly true for an experiment in which the sea surface temperature was raised artificially by 8°C. An intense vortex, featuring winds of minimal hurricane force, developed when the wind speed dependence was retained. Without the wind speed dependence, a more modest low that lacked hurricane force winds evolved. This finding lends strong support to the hypothesis of Emanuel and Rotunno (1989) that air-sea interaction instability (ASII) is a major factor in at least some types of polar low development.

Perhaps a surprising finding was the strong sensitivity of the polar low development to the shape of the upstream ice boundary. Leaving this boundary unchanged but displacing the east shore of Hudson Bay far to the east and vastly enlarging the area of open water, had only a minor effect on the position and intensity of the fully developed low. However, replacing the indented ice boundary by a straight, meridionally oriented boundary resulted in a striking reduction in the intensity of the low and a large displacement in its position. Citing observational findings of Lystad (1986) and modeling results of Grønås et al. (1987), Nordeng (1990) called attention to a propensity for polar low formation in the vicinity of the wedge-shaped region of open water that lies to the west of Spitzbergen and extends southward to Bear Island. Relatedly, a series of polar lows reported by Reed and Duncan (1987) appeared to have their source in this region. Thus it does not seem far-fetched to suggest that the configuration of the ice boundary can have an important influence on polar low formation. Quite possibly, favored positions are determined by the behavior of boundary-layer fronts (Fett, 1989) (also called Arctic fronts; Shapiro et al., 1989) that are common near, and propagate outward from, the ice edge. Relatedly, Andersson and Gustafsson (1994) have shown the importance of the shape of the coast in the formation of convective snowbands that appear over the Baltic Sea during cold outbreaks.

Numerous studies have implicated baroclinicity in the formation of polar lows, either through the agency of shallow "Arctic" fronts, as in the abovecited articles of Reed and Duncan (1987), Shapiro et al. (1989), and Fett (1989), or in connection with upper-level mobile troughs that give rise to upward motions and attendant large-scale destabilization and condensation heating. Baroclinic effects are particularly important in the formation of what Rasmussen (1983) has termed the comma cloud type of polar low (Reed, 1979; Reed and Blier, 1986). Nordeng (1990) and Montgomery and Farrell (1992) envisage polar low formation to entail two phases: a development phase in which baroclinic forcing, as expressed, for instance, by the advection of vorticity by the thermal wind, initiates the spin-up and a diabatic destabilization or convective phase that maintains and strengthens the development. Nordeng and Rasmussen (1992), in a similar vein, refer to baroclinic energy release as the triggering mechanism of polar lows and latent heat release as the main driving mechanism. Craig and Cho (1989) have also considered baroclinic instability to constitute one of two driving mechanisms for polar lows and comma clouds.

The question arises whether baroclinic influences, either in the form of energy release from a baroclinically unstable Arctic front or of forced lifting by an upper-level, short-wave trough, were important elements in the initiation of the polar low under investigation. First, with respect to boundary-layer fronts, it seems questionable to characterize the elliptical zone of temperature contrast along the border of the open water (Fig. 2a) as a front that relates to the problem of baroclinic instability. Indeed, in the experiment (HB3) that was started without this feature, the zone quickly formed as a consequence of the intense sensible heat flux. It seems more logical to attribute the development in this case to the fluxes, and the associated latent heat release in deep convection, than to a baroclinic instability of the shallow, flux-induced thermal gradient. Second, as regards forcing by an upper-level mobile trough, such a feature did indeed exist (Figs. 2c, 4c), and gives the appearance of constituting a potentially significant triggering mechanism. However, the same feature existed in the ice-covered experiment in which a surface low failed to develop. Clearly, the upper-level baroclinic forcing *by itself* was insufficient to initiate a surface low.

The latter conclusion must be tempered by the fact that the ice-covered experiment, in order to be consistent with a totally ice-covered state, employed an artificially enhanced static stability below 700 mb. As shown by Hoskins et al. (1985) the effectiveness of an upper-level disturbance (positive potential vorticity (PV) anomaly) in inducing a surface cyclone depends inversely on the static stability of the intervening layer. Thus, forcing by the upper-level trough might have exerted some influence on the surface development had the true static stability been used. But the weakness of the development in experiment HB5, which employed the true initial stability and allowed for its later reduction by sensible heat flux, suggests that the effect was small.

In view of the evidence that baroclinic forcing by the upper-level trough had at most a small effect on the surface development, it must be asked what feature of the upper-level flow was conducive to the deepening, since it seems unlikely that the polar low and cold low aloft appeared together by coincidence. It is our suggestion that the general cooling aloft accompanying the advance of the upper-level cold low (Fig. 4d), was the key factor. This cooling, coupled with low-level warming and moistening by the surface fluxes, resulted in a drastic destabilization of the layer between the surface and 550 mb, as witnessed by the difference in the beginning (Fig. 8, dashed lines) and ending (Fig. 8, solid lines) soundings at the position of the low center. From the point of view of the sensitivity experiments the destabilization gave rise to substantial condensation heating in deep mesoscale convection, and from the point of view of potential vorticity diagnostics it allowed a large, mid-level, positive PV anomaly (not shown) to induce cyclonic flow all the way to the surface. In support of the destabilization argument, it is noted that Businger (1985) has shown statistically that upper-level cold lows are the favored locale for polar lows, and Rasmussen et al. (1992) have emphasized the importance of an upper-level cold dome in the formation of a well-documented polar low that formed between Bear Island and Norway in December 1982. As shown by these authors, the low formed beneath the region of coldest temperatures aloft. The PV argument is admittedly speculative and requires confirmation by a quantitive procedure such as that employed by Davis and Emanuel (1991).

In conclusion, the Hudson Bay case provides an example of polar low development in which baroclinicity appears to have played a minor role. Condensation heating in deep convection was the overwhelming cause of the intensification, and the growth of the convection was a consequence of the concurrent warming and moistening of the lower layers by the surface fluxes and the simultaneous cooling of the layers above by the advance of the upper-level cold low. In the inferred absence, or near absence, of baroclinic forcing as a triggering and organizing mechanism, there is evidence that the configuration of the ice boundary played an important role in focusing the development.

6. Acknowledgments

We wish to express our gratitude to Ying-Hwa Kuo for his encouragement and advice, to Richard Rotunno, Christopher Davis, and Simon Low-Nam for helpful comments, to Candace Gudmundson for editorial assistance, to Kay Dewar for assistance in figure preparation, and to Christine Rice, Lara Braithwaite and Hilary Price for manuscript preparation. The critical comments and helpful suggestions of an anonymous reviewer are also gratefully acknowledged. This research was supported by the National Science Foundation under grant ATM-9213851.

REFERENCES

Andersson, T. and Gustafsson, N. 1994. Coast of departure and coast of arrival: Two important concepts for the formation and structure of convective snowbands over seas and lakes. *Mon. Wea. Rev.* **122**, 1036–1049.

Arakawa, A. and Schubert, W. H. 1974. Interaction of a cumulus cloud ensemble with the large scale environment, Part I. *J. Atmos. Sci.* **31**, 674–701.

Blackadar, A. K. 1979. High-resolution models of the planetary boundary layer. In: *Advances in Environmental Science and Engineering* **1**, no. 1 (eds. Pfafflin and Zeigler). Gordon and Breach Sci. Publ., New York, 50–85.

Businger, S. 1985. The synoptic climatology of polar low outbreaks. *Tellus* **37A**, 419–432.

Craig, G. and Cho, H.-R. 1989. Baroclinic instability and CISK as the driving mechanisms for polar lows and comma clouds. In: *Polar and arctic lows* (eds. P. F. Twitchell, E. A. Rasmussen and K. L. Davidson). A. Deepak Publishing, Virginia, USA, 131–140.

Davis, C. A. and Emanuel, K. A. 1991. Potential vorticity diagnostics of cyclogenesis. *Mon. Wea. Rev.* **199**, 1929–1953.

Emanuel, K. A. and Rotunno, R. 1989. Polar lows as Arctic hurricanes. *Tellus* **41A**, 1–17.

Fett, R. W. 1989. Polar low development associated with boundary-layer fronts in the Greenland, Norwegian and Barents Seas. In: *Polar and arctic lows* (eds. P. F. Twitchell, E. A. Rasmussen and K. L. Davidson). A. Deepak Publishing, Virginia, USA, 313–322.

Grell, G. A. 1993. Prognostic evaluation of assumptions used by cumulus parameterizations. *Mon. Wea. Rev.* **121**, 764–787.

Grønås, S., Foss, A. and Lystad, M. 1987. Numerical simulations of polar lows in the Norwegian Sea. *Tellus* **39A**, 334–354.

Hoskins, B. J., McIntyre, M. E. and Robertson, A. W. 1985. On the use and significance of isentropic potential vorticity maps. *Quart. J. Roy. Meteor. Soc.* **111**, 877–946.

Hsie, E.-Y., Anthes, R. A. and Keyser, D. 1984. Numerical simulation of frontogenesis in a moist atmosphere. *J. Atmos. Sci.* **41**, 2581–2594.

Lystad, M. 1986. Polar lows in the Norwegian, Greenland and Barents Sea. *Final Report of the Polar Lows Project*. The Norwegian Meteorological Institute, P.O. Box 43—Blindern, 0313 Oslo 3, Norway.

Montgomery, M. T. and Farrell, B. F. 1992. Polar low dynamics. *J. Atmos. Sci.* **49**, 2484–2505.

Nordeng, T. E. 1990. A model-based diagnostic study of the development and maintenance mechanism of two polar lows. *Tellus* **42A**, 92–108.

Nordeng, T. E. and Rasmussen, E. A. 1992. A most beautiful polar low. A case study of a polar low development in the Bear Island region. *Tellus* **44A**, 81–99.

Økland, H. 1987. Heating by organized convection as a source of polar low intensification. *Tellus* **37A**, 397–407.

Rasmussen, E. 1983. A review of mesoscale disturbances in cold air masses. In: *Mesoscale meteorology-theories, observations and models* (eds. D. K. Lilly and T. Gal-Chen). D. Reidel Publishing Company, Boston, 247–283.

Rasmussen, E. A., Padersen, T. S., Pedersen, L. T. and Turner, J. 1992. Polar lows and arctic instability lows in the Bear Island region. *Tellus* **44A**, 133–154.

Reed, R. J. 1979. Cyclogenesis in polar air streams. *Mon. Wea. Rev.* **107**, 38–52.

Reed, R. J. and Blier, W. 1986. A case study of comma cloud development in the eastern Pacific. *Mon. Wea. Rev.* **114**, 1681–1695.

Reed, R. J. and Duncan, C. N. 1987. Baroclinic instability as a mechanism for the serial development of polar lows: A case study. *Tellus* **39A**, 376–384.

Roch, M., Benoit, R. and Parker, N. 1991. Sensitivity experiments for polar low forecasting with the CMC mesoscale finite-element model. *Atmos.-Ocean* **29**, 381–419.

Shapiro, M. A., Hampel, T. and Fedor, L. S. 1989. Research aircraft observations of an Arctic front over the Barents Sea. In: *Polar and arctic lows* (eds. P. F. Twitchell, E. A. Rasmussen and K. L. Davidson). A. Deepak Publishing, Virginia, USA, 279–290.